Orthogonality catastrophe and Kondo effect in graphene

Martina Hentschel
Max-Planck-Institut für Physik komplexer Systeme, Nöthnitzer Strasse 38, D-01187 Dresden, Germany

Francisco Guinea
Instituto de Ciencia de Materiales de Madrid, CSIC, Sor Juana Inés de la Cruz 3, E-28049 Madrid, Spain
(Received 3 May 2007; revised manuscript received 2 July 2007; published 10 September 2007)

Anderson's orthogonality catastrophe [Phys. Rev. Lett. **18**, 1049 (1967)] in graphene, at energies close to the Dirac point, is analyzed. It is shown that, in clean systems, the orthogonality catastrophe is suppressed due to the vanishing density of states at the Dirac point. In the presence of preexisting localized states at the Dirac energy, the orthogonality catastrophe shows features similar to those found in normal metals with a finite density of states at the Fermi level. The implications for the Kondo effect induced by magnetic impurities, and for the Fermi edge singularities in tunneling processes, are also discussed.

DOI: 10.1103/PhysRevB.76.115407 PACS number(s): 73.20.Hb, 73.23.−b, 72.15.Qm

I. INTRODUCTION

Graphene has attracted a great deal of attention recently due to its novel fundamental properties and potential applications.[1–5] It is, by now, well established that its electronic properties at low energies are well described by the two-dimensional Dirac equation. At half filling, graphene should be a semimetal, with a vanishing density of states. This fact implies that many properties of a metal, which are parametrized by the density of states at the Fermi level, are different in a clean graphene sample. The description of the electronic bands in graphene based on the Dirac equation also leads to localized states in samples with edges[6,7] or lattice defects.[8,9] These states change the density of states near the Dirac energy, as they induce a peak at this energy. Hence, the density of states of graphene at the Dirac energy can either vanish, in a clean sample, or diverge, if localized states are induced.

We study here Anderson's orthogonality catastrophe[10] (AOC) in clean and dirty graphene. The AOC can be considered the simplest nontrivial feature in the response of a metal, and it is dependent on the value of the density of states at the Fermi level. The AOC directly leads to many singularities in experiments which probe the dynamical response of a metal, like the Fermi edge singularity in x-ray absorption[11,12] and singularities in the optical and transport properties of quantum dots and metallic grains.[13–16] In graphene, the interplay between the AOC and Coulomb blockade may be relevant for the analysis of transport experiments on small quantum dots.[5,17]

The Kondo effect induced by magnetic impurities in metals can be seen as a direct consequence of Anderson's orthogonality catastrophe.[18,19] The coupling between the impurity spin and the conduction electrons can be divided into a transverse term, $J_\perp$, which leads to spin-flip processes, and a longitudinal term, $J_\parallel$, which induces an AOC associated with the same spin flips. This AOC leads to a strong suppression of spin fluctuations, although the effects of $J_\perp$ prevail at the lowest temperatures. These two competing processes can be defined, in a very transparent way, in the dissipative two level system,[20] which is equivalent to the Kondo Hamiltonian. The Kondo temperature T_K can be seen as the scale at which spin-flip processes ultimately cut off the AOC. The formation of a Kondo singlet in semimetallic systems was studied in Refs. 21 and 22. The vanishing of the density of states at the Fermi level leads to the suppression of the Kondo effect and to the existence of a quantum phase transition above a finite value of the exchange coupling. The relevance of the energy dependent density of states for the Kondo effect in graphene was pointed out in Ref. 23.

The AOC is modified in disordered metals[24] and ballistic mesoscopic systems due to the changes in the electronic wave functions.[25,26] We will analyze the AOC in graphene using the numerical methods explained in Refs. 25 and 26 (see also Ref. 27) and also a phase shift analysis similar to that in Ref. 10.

We analyze first the phase shifts induced by a local potential, first in clean graphene and then in graphene in the presence of preexisting localized levels. The next section presents a numerical study of the full overlap between the electronic ground state before and after the potential is turned on, and an analysis of the scaling of this quantity with system size. The last section discusses the main implications of our work for the Kondo effect in graphene, and the Fermi edge singularities associated with tunneling processes.

II. PHASE SHIFT ANALYSIS

The overlap S between the Slater determinants which describe the electronic wave function before and after a potential is switched on can be written as[10]

$$S \leqslant N \exp\left[-\sum_l \frac{2l+1}{3\pi^2} \sin^2(\delta_l)\right], \tag{1}$$

where N is the number of electrons and δ_l is the phase shift induced by the potential in the scattered waves at the Fermi level with angular momentum l. In a typical metal, a weak local potential of strength $\epsilon_0 \ll \epsilon_F$ induces a phase shift in the s channel which can be approximated by $\delta_0 \approx \epsilon_0 N(\epsilon_F) \ll 1$, where $N(\epsilon_F)$ is the density of states at the Fermi level.

 ©2007 The American Physical Society

This analysis can be extended in a straightforward way to graphene, where the electronic wave functions can be approximated by the two-dimensional Dirac equation (see below):

$$\mathcal{H} \equiv v_F \begin{pmatrix} 0 & \pm k_x + i k_y \\ \mp k_x + i k_y & 0 \end{pmatrix}, \tag{2}$$

where the two signs correspond to the two inequivalent corners of the Brillouin zone of the honeycomb lattice.

We use Eq. (1) in order to describe the dependence of the overlap on the number of electrons, by computing analytically the phase shifts induced by different types of potentials. In the following, we use energy and momentum units such that $v_F = 1$.

A. Clean graphene

We analyze first the phase shifts induced by a circular potential well in clean graphene, and we describe the electronic wave functions using the continuum Dirac equation [Eq. (2)]. We expect that this approximation will describe qualitatively the effects of a local perturbation in the graphene lattice.

We assume that the potential well can scatter electrons between the K and K' valleys, as is the case for sufficiently localized potentials in graphene.

Using cylindrical coordinates, the Hamiltonian in the clean system can be written as

$$\mathcal{H} \equiv \begin{pmatrix} 0 & i e^{-i\phi} \partial_r + \frac{e^{-i\phi}}{r} \partial_\phi & 0 & 0 \\ i e^{i\phi} \partial_r - \frac{e^{-i\phi}}{r} \partial_\phi & 0 & 0 & 0 \\ 0 & 0 & 0 & -i e^{i\phi} \partial_r + \frac{e^{i\phi}}{r} \partial_\phi \\ 0 & 0 & -i e^{-i\phi} \partial_r - \frac{e^{-i\phi}}{r} \partial_\phi & 0 \end{pmatrix}, \tag{3}$$

where the two first entries correspond to the K point, and the two last ones to the K' point.

We add a constant perturbation in the region $r \leqslant R_0$:

$$V \equiv \begin{pmatrix} \epsilon_0 & 0 & 0 & \Delta \\ 0 & \epsilon_0 & \Delta & 0 \\ 0 & \Delta & \epsilon_0 & 0 \\ \Delta & 0 & 0 & \epsilon_0 \end{pmatrix}, \tag{4}$$

where ϵ_0 is a constant energy shift and Δ is a potential which induces scattering between the two valleys, and it is compatible with the symmetries of the honeycomb lattice.[28]

We analyze the scattering of an incident s wave with incoming energy k:

$$\Psi_{\text{inc}}(r,\phi) \equiv \begin{pmatrix} J_0(kr) \\ -i J_1(kr) e^{i\phi} \\ 0 \\ 0 \end{pmatrix}, \tag{5}$$

where $J_0(x)$ and $J_1(x)$ are Bessel functions of the first kind. They satisfy $\lim_{x\to 0} J_0(x) \approx 1$ and $\lim_{x\to 0} J_1(x) \approx x/2$.

The reflected waves outside the well can be written as

$$\Psi_{\text{ref}}(r,\phi) \equiv R_1 \begin{pmatrix} Y_0(kr) \\ -i Y_1(kr) e^{i\phi} \\ 0 \\ 0 \end{pmatrix} + R_2 \begin{pmatrix} 0 \\ 0 \\ i Y_1(kr) e^{i\phi} \\ Y_0(kr) \end{pmatrix}. \tag{6}$$

$Y_0(x)$ and $Y_1(x)$ are Bessel functions of the second kind. They satisfy $\lim_{x\to 0} Y_0(x) \approx 2/\pi [\log(x/2) + \gamma]$ and $\lim_{x\to 0} Y_1(x) \approx -2/(\pi x)$. The first contribution on the right hand side of Eq. (6) is a reflected wave in the same valley, and the second term is a wave in the opposite valley as the incident wave.

Inside the potential well, the spectrum has a gap for energies $\epsilon_0 - \Delta \leqslant \epsilon \leqslant \epsilon_0 + \Delta$. Within this range of energies, the wave function inside the well can be written as

$$\Psi_{\text{trans}}(r,\phi) \equiv T_1 \begin{pmatrix} \frac{\sqrt{\Delta^2-k'^2}}{\sqrt{2}\Delta} I_0(k'r) \\ +i\frac{k'}{\sqrt{2}\Delta} I_1(k'r)e^{i\phi} \\ 0 \\ \frac{1}{\sqrt{2}} I_0(k'r) \end{pmatrix} + T_2 \begin{pmatrix} \frac{ik'}{\sqrt{2}\Delta} I_0(k'r) \\ \frac{\sqrt{\Delta^2-k'^2}}{\sqrt{2}\Delta} I_1(k'r)e^{i\phi} \\ i\frac{1}{\sqrt{2}} I_1(k'r)e^{i\phi} \\ 0 \end{pmatrix}. \quad (7)$$

$I_0(x)$ and $I_1(x)$ are modified Bessel functions of the first kind. They satisfy $\lim_{x\to 0} I_0(x) \approx 1$ and $\lim_{x\to 0} I_1(x) \approx x/2$. The value of k' in Eq. (7) is given by $\epsilon = \sqrt{\Delta^2 - k'^2}$. As $k = \epsilon + \epsilon_0$, we have $k' = \sqrt{\Delta^2 - (k-\epsilon_0)^2}$.

For $|\epsilon - \epsilon_0| \geq \Delta$, we have

$$\Psi_{\text{trans}}(r,\phi) \equiv T_1 \begin{pmatrix} \frac{1}{\sqrt{2}\Delta} J_0(k'r) \\ -i\frac{\Delta}{\sqrt{2(\Delta^2+k'^2)}} J_1(k'r)e^{i\phi} \\ 0 \\ \frac{\Delta}{\sqrt{2(\Delta^2+k'^2)}} J_0(k'r) \end{pmatrix} + T_2 \begin{pmatrix} \frac{i\Delta}{\sqrt{2(\Delta^2+k'^2)}} J_0(k'r) \\ \frac{1}{\sqrt{2}} J_1(k'r)e^{i\phi} \\ \frac{\Delta}{\sqrt{2(\Delta^2+k'^2)}} J_1(k'r)e^{i\phi} \\ 0 \end{pmatrix}, \quad (8)$$

and $\epsilon = \sqrt{\Delta^2 + k'^2}$ and $k' = \sqrt{(k-\epsilon_0)^2 - \Delta^2}$.

The scattering phase shifts are determined by the reflection coefficients R_1 and R_2 defined in Eq. (6). The boundary conditions at $r = R_0$ are simply the continuity of the spinors, which define a set of four equations for the four variables R_1, R_2, T_1, and T_2.

For $\Delta = 0$, we have $R_2 = T_2 = 0$ and $R_1 = \bar{R}$. As $\lim_{x\to\infty} J_0(x) \approx \sqrt{2/(\pi x)} \cos(x - \pi/4)$ and $\lim_{x\to\infty} Y_0(x) \approx \sqrt{2/(\pi x)} \sin(x - \pi/4)$, the phase shift δ is $\tan\delta = \bar{R}$. We find

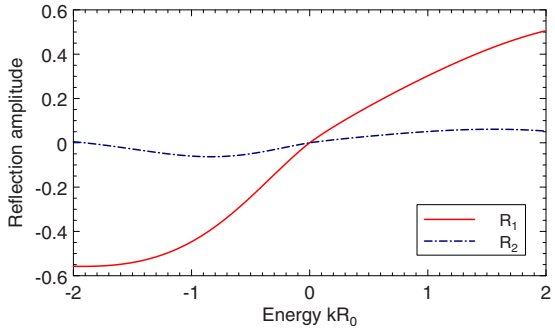

FIG. 1. (Color online) Reflection coefficients R_1 and R_2 [solid and broken lines, cf. Eq. (6)] of a circular well with $\epsilon_0 R_0 = 0.5$ and $\Delta R_0 = 0.1$.

$$\tan\delta = \bar{R}(kR_0) = -\frac{J_1[(k-\epsilon_0)R_0]J_0(kR_0) - J_0[(k-\epsilon_0)R_0]J_1(kR_0)}{J_1[(k-\epsilon_0)R_0]Y_0(kR_0) - J_0[(k-\epsilon_0)R_0]Y_1(kR_0)} \quad (9)$$

and

$$\lim_{kR_0\to\infty} \bar{R}(kR_0) = \tan(\epsilon_0 R_0). \quad (10)$$

Results for $\epsilon_0 R_0 = 0.5$ and $\Delta R_0 = 0.1$ are shown in Fig. 1. In all cases, with or without [Eq. (9)] intervalley scattering, the reflection coefficients vanish at the Dirac point, $k = 0$. This result can be simply understood by noting that a finite reflection coefficient implies a reflected wave function with a component $Y_1(kr)$, which diverges as $k \to 0$. The phase shift vanishes linearly as $k \to 0$, in agreement with general arguments based on the vanishing of the density of states at the Dirac point.

The vanishing of the phase shift at the Dirac point implies that the overlap between the Slater determinants before and after the potential is switched on does not scale like some power of the number of electrons, and the AOC does not take place at this energy.

B. Phase shift analysis in the presence of a localized state

Next, we study the phase shifts induced by a weak potential near the edges of a circular void which supports surface states. A sketch of the model is shown in Fig. 2. We will neglect intervalley scattering terms, which is justified even for impurities of an extension of the order equal to or larger than the lattice spacing. This can be seen easily by a straightforward approximation of the impurity by a Gaussian and subsequent Fourier transformation to reciprocal space.[29] The wave function can, thus, be written as

$$\Psi(\tilde{\mathbf{r}}) \equiv \begin{pmatrix} \psi_1(\tilde{\mathbf{r}}) \\ \psi_2(\tilde{\mathbf{r}}) \end{pmatrix}. \quad (11)$$

The edge of a crack, or extended vacancy, is modeled by the boundary condition:

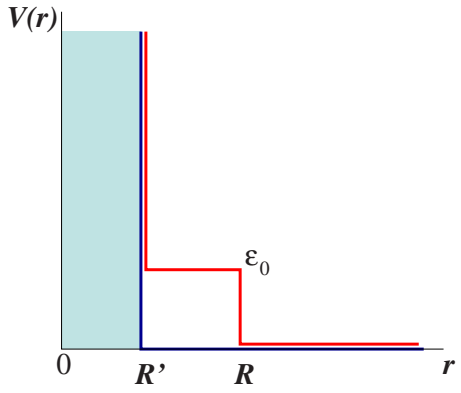

FIG. 2. (Color online) Sketch of the model with circular symmetry used to study the AOC in the presence of localized levels. An infinite potential exists for $0 \leqslant r \leqslant R'$, mimicking a vacancy. The perturbation leading to the AOC is modeled as a constant potential, ϵ_0, for $R' \leqslant r \leqslant R$ (see text for details).

$$\psi_1(\tilde{\mathbf{r}}) = 0, \quad \tilde{\mathbf{r}} \in \Omega, \tag{12}$$

where Ω is the boundary of the void.

We analyze a circular void of radius R'. The boundary condition [Eq. (12)] allows for solutions at zero energy of the type

$$\Psi(\tilde{\mathbf{r}}) \equiv \begin{pmatrix} 0 \\ \dfrac{e^{\pm in\theta}}{r^n} \end{pmatrix}, \tag{13}$$

where the two signs correspond to the two inequivalent corners of the Brillouin zone.

Equation (12) implies, for s-wave scattering,

$$\alpha_0 J_0(kR') + \beta_0 Y_0(kR') = 0. \tag{14}$$

The phase shift induced by the void, before the potential whose effect we want to calculate is turned on, is (see also Ref. 30)

$$\delta_0(k) = \arctan\left(\frac{\beta_0}{\alpha_0}\right) = -\arctan\left(\frac{J_0(kR')}{Y_0(kR')}\right) \xrightarrow{k\to 0} -\frac{\pi}{2}\frac{1}{\ln(kR')}. \tag{15}$$

Next, we model a weak impurity near the void as an isotropic perturbation of depth ϵ_0, defined in the region $R' \leqslant |\tilde{\mathbf{r}}| \leqslant R$. Following Eqs. (5) and (6) and neglecting intervalley scattering, the wave function can be written as

$$\Psi(\tilde{\mathbf{r}}) \equiv \begin{cases} \begin{pmatrix} \alpha' J_0[(k+\epsilon_0)r] + \beta' Y_0[(k+\epsilon_0)r] \\ \alpha' J_1[(k+\epsilon_0)r]e^{i\phi} + \beta' Y_1[(k+\epsilon_0)r]e^{i\phi} \end{pmatrix}, & R' \leqslant r \leqslant R \\ \begin{pmatrix} \alpha J_0(kr) + \beta Y_0(kr) \\ \alpha J_1(kr)e^{i\phi} + \beta Y_1(kr)e^{i\phi} \end{pmatrix}, & R \leqslant r, \end{cases} \tag{16}$$

with boundary conditions

$$\alpha' J_0[(k+\epsilon_0)R'] + \beta' Y_0[(k+\epsilon_0)R'] = 0,$$

$$\alpha' J_0[(k+\epsilon_0)R] + \beta' Y_0[(k+\epsilon_0)R] = \alpha J_0(kR) + \beta Y_0(kR),$$

$$\alpha' J_1[(k+\epsilon_0)R] + \beta' Y_1[(k+\epsilon_0)R] = \alpha J_1(kR) + \beta Y_1(kR). \tag{17}$$

These equations allow us to obtain the phase shift of the combined system, void and circular impurity, as $\delta = \arctan(\beta/\alpha)$. The overlap between the Slater determinants before and after the impurity potential is switched on is determined by the phase difference, $\delta - \delta_0$, where δ_0 is given in Eq. (15).

Results for the individual phase shifts δ and δ_0, as well as their difference, are shown in Fig. 3 for $\epsilon_0 = 0.1, R' = 0.9$, and $R = 1$. In the regime of energies much lower than ϵ_0, the phase shift δ seems to approach δ_0 from below, indicating that the repulsive character of the void is weakened by the additional constant potential. For the small energies close to the Dirac point focused on here, the relative phase shift, $\delta - \delta_0$, is always finite and seems to approach a constant. This behavior differs strikingly from our findings for clean graphene, where the vanishing of the phase shift at the Dirac point (cf. Fig. 1) indicates the suppression of AOC. In the presence of voids, the small dependence of the phase shift

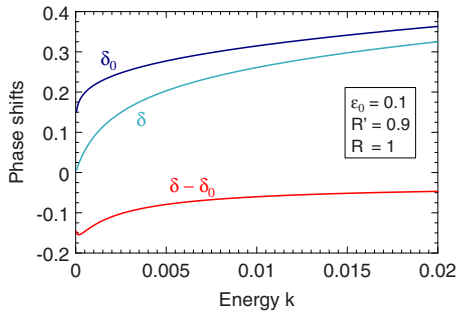

FIG. 3. (Color online) Phase shift δ_0 induced by a void, the phase shift δ resulting from the additional switching on of a constant potential, and the resulting relative phase shift $\delta - \delta_0$ induced by a circular impurity potential surrounding a void (see text for details).

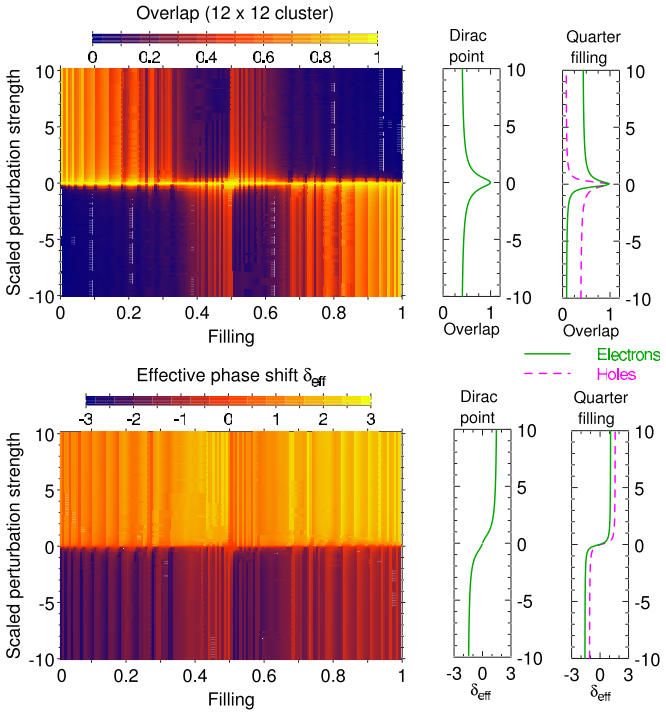

FIG. 4. (Color online) Overlap and effective phase shift as function of filling and potential strength (see text for details).

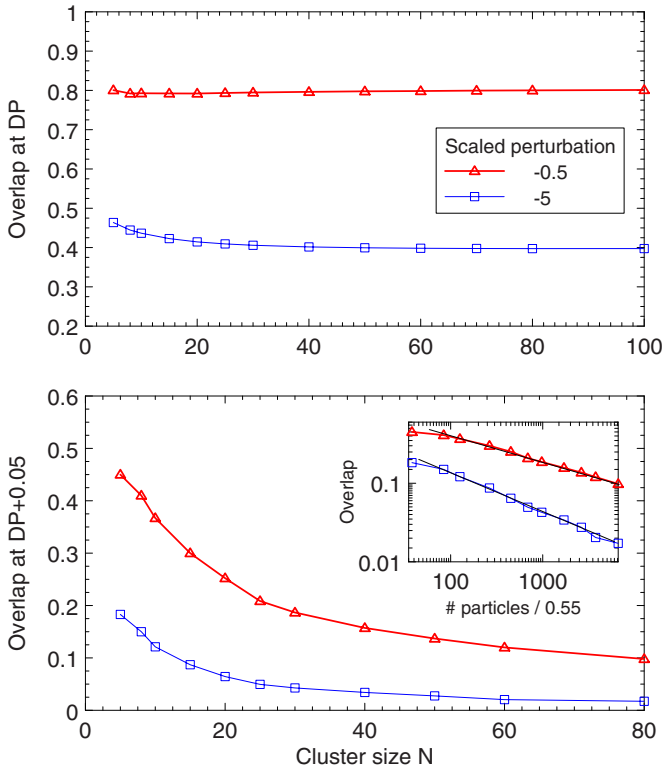

FIG. 5. (Color online) Scaling of the overlap with cluster size N at the Dirac point (DP, $\epsilon_F=0$, corresponding to a filling of 0.5; top panel) and away from the Dirac point (at fixed filling 0.55, corresponding to $\epsilon_F \sim 0.67$; lower panel). See text for details.

induced by an additional external potential on energy near the Dirac point implies that the overlap between Slater determinants should scale with the number of electrons in a similar fashion to that in a normal metal with a finite density of states. We shall see in the remainder of this paper that there are, indeed, considerable differences between clean graphene and graphene with localized states that are visible, e.g., in the behavior of the AOC overlap.

III. CALCULATION OF THE OVERLAP

A. Clean graphene

The overlap between the unperturbed and perturbed Slater determinants for clean graphene clusters of different sizes has been calculated using the methods described in Refs. 25–27. The perturbation is a local potential at a given site, $\Delta=\epsilon_0$. Its strength is measured in terms of the scaled perturbation strength $\propto\Delta/d$, with d being the mean level spacing, $6/[(N(N+1)-2)]$. Periodic boundary conditions are used in systems with $N\times N$ unit cells, up to $N=80$; the vertical stripes visible in Fig. 4 are an artifact of the periodic boundary conditions. The results for the overlap for $N=12$ and different potential strengths (ranging from weak to strong for repulsive as well as attractive perturbations) are shown in Fig. 4. An effective phase shift can be defined by dividing the energy shift of the level closest to the Fermi energy by the average level spacing in that energy range. This phase shift is also shown in Fig. 4.

The dependence of the overlap with system size is different at the Dirac point from that at other energies. This dependence is shown in Fig. 5. The overlap is almost independent of system size at the Dirac point (cf. the upper panel). This result is consistent with the phase shift analysis, which shows that the phase shift vanishes at the Dirac point. Indeed, AOC is suppressed at the Dirac point. Away from the Dirac point, the conventional behavior of the AOC overlap is recovered (see the lower panel of Fig. 5). To this end, AOC overlaps for fillings ranging from 0.54 to 0.56 were averaged over. Clearly, the AOC overlap is no longer suppressed and approaches zero in the thermodynamic limit following the well-known power-law dependence on the number of particles ($\propto[N(N+1)-2]$, cf. inset of Fig. 5).

B. Graphene with localized states

The method described in Ref. 27 assumes that the wave functions of all eigenstates of the unperturbed system have the same weight on the site where the perturbation is turned on. This leads to a considerable simplification of the calculation of the overlap between Slater determinants. Generalization of this method to chaotic mesoscopic systems[13,25,26] was done based on the statistical properties of the chaotic wave functions.

In the presence of a defect which induces a localized state, like a vacancy, the wave functions of the unperturbed state, where the localized state is already present, do not possess translational symmetry. Therefore direct diagonalization and calculation of the overlap determinants were used for the study of clusters of moderate sizes.

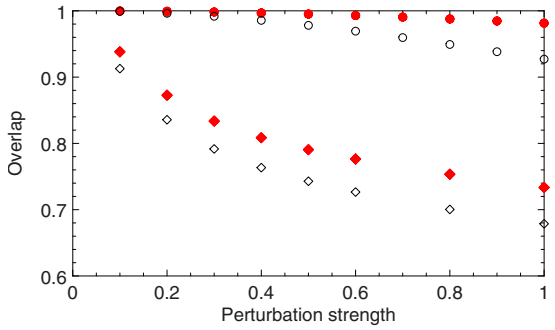

FIG. 6. (Color online) Dependence of the overlap on perturbation strength when the perturbation is turned on near an existing vacancy (empty circles, black) and in clean graphene (filled circles, red). Calculations are done for 12×12 clusters. Circles correspond to one hole in the cluster (Dirac energy, $\epsilon_F=0$), whereas diamonds characterize a cluster with five holes (corresponding to $\epsilon_F=-0.5$ or a filling of ~0.47).

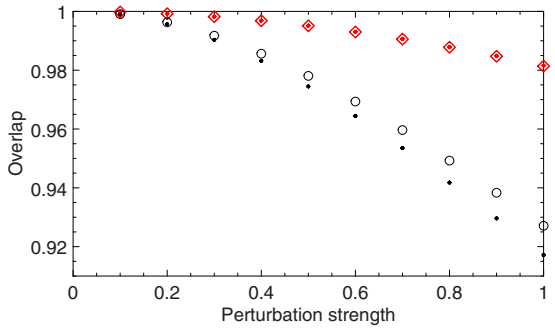

FIG. 7. (Color online) Dependence of the overlap on perturbation strength, at the Dirac energy, when the perturbation is turned on near an existing vacancy (circles, black) and in clean graphene (diamonds, red). Large symbols correspond to a 12×12 cluster and small symbols correspond to a 15×15 cluster.

Results for the overlap for clusters with 12×12 unit cells are shown in Fig. 6. At the Dirac point, the presence of a vacancy, which induces a localized state, enhances significantly the dependence of the overlap on the strength of the potential. Away from the Dirac point, the difference in the overlap with and without a vacancy is much less pronounced. We show in Fig. 7 the dependence of the overlap with cluster size at the Dirac energy. As anticipated in the discussion of Fig. 3, the presence of a vacancy near the potential which is turned on modifies significantly the results in comparison with a clean system. In the latter, the dependence on size is negligible, in agreement with the results shown in Fig. 5. There is, on the other hand, a substantial dependence on cluster size when a vacancy induces a localized state at the Dirac energy.

IV. KONDO EFFECT

The anisotropic Kondo Hamiltonian reads

$$\mathcal{H}_K = \sum_{k,s} \epsilon_k c^\dagger_{k,s} c_{k,s} + J_\parallel S_z \sum_{k,k'} (c^\dagger_{k,\uparrow} c_{k',\uparrow} - c^\dagger_{k,\downarrow} c_{k',\downarrow}) + J_\perp \sum_{k,k'} S^+ c^\dagger_{k,\downarrow} c_{k',\uparrow} + \text{H.c.} \quad (18)$$

For $J_\perp=0$, the model is exactly solvable and the ground state is twofold degenerate, with a well defined value of S_z. For $S_z=+1$, for instance, the electronic wave function is the product of two Slater determinants, one for each spin component, which describe the ground state of noninteracting electrons in a local potential of magnitude $\pm J_\parallel$.

The overlap between the ground state wave functions which correspond to $S_z=+1$ and $S_z=-1$, $S_{+-N}=\langle+N|-N\rangle$, is given by the product of the individual overlaps for each spin species because these are not coupled. These overlaps can be expressed in terms of the phase shifts induced by the potential $\pm J_\parallel$, $\delta_0 \equiv \delta_{\pm J_\parallel}$ and $\delta_{l>0}=0$. In a metal, these overlaps tend to zero as $N\to\infty$ as $S_{+-N}\sim N\exp[-2\sin^2(\delta_{\pm J_\parallel})/(3\pi^2)]$.

Alternatively, one can take an approach motivated by a renormalization group analysis and define a hopping related, energy dependent overlap, $s_{+-\epsilon}$, where only electronic states with energies ϵ above the Fermi energy are included. This overlap scales as $s_{+-\epsilon}\sim(|\epsilon|/\Lambda)\exp[2\sin^2(\delta_{\pm J_\parallel})/(3\pi^2)]$ with energy, where Λ is a high-energy cutoff of the order of the bandwidth or the range of validity of the Kondo Hamiltonian. Expressing this scaling behavior in terms of $N_\epsilon \sim |\epsilon|^{-1}$, it becomes evident that the scaling with N is the same as that for the Anderson overlap discussed before.

The Kondo effect arises because spin-flip processes, induced by $J_\perp$, suppress the orthogonality catastrophe described above, which, in turn, modifies $J_\perp$. The low-energy properties of the Kondo model can be mapped onto bosonic and electronic models which describe the competition between quantum fluctuations and decoherence effects due to Anderson's orthogonality catastrophe.[20,31] The simplest such model is the dissipative two level model, which describes a quantum two level system interacting with a dissipative environment,[32,33] which has been extensively studied.[34,35] The main physical difference between the Kondo model and the dissipative two level model is the fact that a spin flip requires the transfer of an electron from one spin channel to the other. This situation is similar to the combination of orthogonality catastrophe and the excitonic instability found in x-ray absorption.[11,12] Because of it, the relevant divergences are proportional to $\sin(\delta_{\pm J_\parallel})$ and not to $\sin^2(\delta_{\pm J_\parallel})$, as in Anderson's orthogonality catastrophe and the ordinary dissipative two level system. Finally, the dimensionless parameter $J\rho(\epsilon_F)$ which characterizes the Kondo temperature, $T_K \propto e^{-c/[J\rho(\epsilon_F)]}$, can be written in terms of the scattering phase shifts as $J\rho(\epsilon_F)\propto\sin(\delta_{\pm J_\parallel})$.

The previous discussion shows that a knowledge of the phase shifts which determine Anderson's orthogonality catastrophe can be used to estimate the Kondo temperature. The phase shifts in graphene change qualitatively depending on the existence, or not, of midgap states. These states are due to the potential scattering induced by the magnetic impurity whose coupling to the graphene band is considered. In normal metals, the spin independent potential induced by a magnetic impurity plays no role in the formation of the Kondo effect. In graphene at half filling, however, a weak scalar potential leads to a vanishing phase shift so that the

spin of the magnetic impurity remains unscreened. When the potential induced by the impurity is strong enough to induce midgap states, the Kondo effect is restored, and the spin will be bound into a singlet at low temperatures.

V. CONCLUSIONS

The results presented here show the existence of two regimes for Anderson's orthogonality catastrophe in graphene at low fillings, depending on whether there are localized states at the Dirac energy or not. In the absence of localized states, the AOC is suppressed near the Dirac point, in agreement with the vanishing of the density of states at this energy. When localized states are present, the AOC is qualitatively similar to that found in metals with a finite density of states. The latter behavior is a consequence of the fact that, when localized states are sufficiently near the Fermi surface, they contribute to the nonadiabatic response of the electron gas. This situation is unique to graphene, as, in most metallic systems, localized states appear at energies well below the Fermi level.

The features discussed above imply that the Kondo effect in graphene also depends on the strength of the scalar potential induced by the magnetic impurity. If the potential induced on the graphene electrons is weak, as when the magnetic impurity is at some distance of the graphene plane, we expect the formation of a Kondo resonance to be suppressed, and the magnetic impurity will give rise to a free magnetic moment. On the other hand, if the magnetic impurity lies within the graphene plane, it will give rise to a strong scalar potential, and possibly to localized states at the Dirac energy. Then, the Kondo effect will not be suppressed, despite the low density of states in graphene near the Dirac energy.

Similar effects can be expected for the Fermi edge singularities induced by electrons tunneling into or out of graphene quantum dots. The strength of the Fermi edge singularities depends on the existence of localized states in the quantum dot. These states will be induced in graphene dots with sharp and rough edges, where, in addition to Coulomb blockade, the AOC associated with electron tunneling will further suppress the conductance at low voltages.[14,15]

ACKNOWLEDGMENTS

F.G. acknowledges funding from MEC (Spain) through Grant No. FIS2005-05478-C02-01, the European Union Contract No. 12881 (NEST), and CAM (Madrid) through program CITECNOMIK. M.H. thanks Eduardo Mucciolo for helpful discussions and the DFG (Germany) for funding within the Emmy Noether Programme.

[1] K. S. Novoselov, A. K. Geim, S. V. Morozov, D. Jiang, Y. Zhang, S. V. Dubonos, I. V. Gregorieva, and A. A. Firsov, Science **306**, 666 (2004).
[2] C. Berger *et al.*, J. Phys. Chem. B **108**, 19912 (2004).
[3] K. S. Novoselov, A. K. Geim, S. V. Morozov, D. Jiang, M. I. Katsnelson, I. V. Grigorieva, S. V. Dubonos, and A. A. Firsov, Nature (London) **438**, 197 (2005).
[4] Y. Zhang, Y.-W. Tan, H. L. Stormer, and P. Kim, Nature (London) **438**, 201 (2005).
[5] A. K. Geim and K. S. Novoselov, Nat. Mater. **6**, 183 (2007).
[6] M. Fujita, K. Wakabayashi, K. Nakada, and K. Kusakabe, J. Phys. Soc. Jpn. **65**, 1920 (1996).
[7] K. Wakabayashi and M. Sigrist, Phys. Rev. Lett. **84**, 3390 (2000).
[8] M. A. H. Vozmediano, M. P. López-Sancho, T. Stauber, and F. Guinea, Phys. Rev. B **72**, 155121 (2005).
[9] V. M. Pereira, F. Guinea, J. M. B. Lopes dos Santos, N. M. R. Peres, and A. H. Castro Neto, Phys. Rev. Lett. **96**, 036801 (2005).
[10] P. W. Anderson, Phys. Rev. Lett. **18**, 1049 (1967).
[11] P. Nozières and C. T. de Dominicis, Phys. Rev. **178**, 1097 (1969).
[12] G. D. Mahan, *Many Body Physics* (Plenum, New York, 1993).
[13] M. Hentschel, D. Ullmo, and H. U. Baranger, arXiv:0706.2612, Phys. Rev. B (to be published).
[14] M. Ueda and F. Guinea, Z. Phys. B: Condens. Matter **85**, 413 (1991).
[15] E. Bascones, C. P. Herrero, F. Guinea, and G. Schön, Phys. Rev. B **61**, 16778 (2000).
[16] D. A. Abanin and L. S. Levitov, Phys. Rev. Lett. **93**, 126802 (2004).
[17] J. S. Bunch, Y. Yaish, M. Brink, K. Bolotin, and P. L. McEuen, Nano Lett. **5**, 287 (2005).
[18] P. W. Anderson, G. Yuval, and D. R. Hamann, Phys. Rev. B **1**, 4464 (1970).
[19] P. W. Anderson and G. Yuval, J. Phys. C **4**, 607 (1971).
[20] F. Guinea, V. Hakim, and A. Muramatsu, Phys. Rev. B **32**, 4410 (1985).
[21] C. R. Cassanello and E. Fradkin, Phys. Rev. B **53**, 15079 (1996).
[22] C. R. Cassanello and E. Fradkin, Phys. Rev. B **56**, 11246 (1997).
[23] K. Sengupta and G. Baskaran, arXiv:0705.0257v2 (unpublished).
[24] Y. Gefen, R. Berkovits, I. V. Lerner, and B. L. Altshuler, Phys. Rev. B **65**, 081106(R) (2002).
[25] M. Hentschel, D. Ullmo, and H. U. Baranger, Phys. Rev. Lett. **93**, 176807 (2004).
[26] M. Hentschel, D. Ullmo, and H. U. Baranger, Phys. Rev. B **72**, 035310 (2005).
[27] K. Ohtaka and Y. Tanabe, Rev. Mod. Phys. **62**, 929 (1990).
[28] J. L. Mañes, F. Guinea, and M. A. H. Vozmediano, Phys. Rev. B **75**, 155424 (2007).
[29] E. Mucciolo (private communication).
[30] M. I. Katsnelson and K. S. Novoselov, Solid State Commun. **143**, 3 (2007).
[31] V. Hakim, A. Muramatsu, and F. Guinea, Phys. Rev. B **30**, 464 (1984).
[32] S. Chakravarty, Phys. Rev. Lett. **49**, 681 (1982).
[33] A. J. Bray and M. A. Moore, Phys. Rev. Lett. **49**, 1545 (1982).
[34] A. J. Leggett, S. Chakravarty, A. T. Dorsey, M. P. Fisher, A. Garg, and W. Zwerger, Rev. Mod. Phys. **59**, 1 (1987).
[35] U. Weiss, *Quantum Dissipative Systems* (World Scientific, Singapore, 1999).